Self-consistent solution of magnetic and friction energy losses of a magnetic nanoparticle

Santiago Helbig,[1,2,*] Claas Abert,[1,3] Pedro A. Sánchez,[1,3,4] Sofia S. Kantorovich,[1,3,5] and Dieter Suess[1,3]

[1]*Faculty of Physics, University of Vienna, Boltzmanngasse 5, 1090 Vienna, Austria*

[2]*Vienna Doctoral School in Physics, University of Vienna, Boltzmanngasse 5, 1090 Vienna, Austria*

[3]*Research Platform MMM Mathematics-Magnetism-Materials, University of Vienna, Oskar-Morgenstern-Platz 1, 1090 Vienna, Austria*

[4]*Physics Department, University of the Balearic Islands, 07122 Palma de Mallorca, Spain*

[5]*Institute of Mathematics and Natural Sciences, Ural Federal University, Lenin av. 51, 620000 Ekaterinburg, Russian Federation*

(Received 11 May 2022; revised 11 November 2022; accepted 17 January 2023; published 16 February 2023)

We present a simple simulation model for analyzing magnetic and frictional losses of magnetic nanoparticles in viscous fluids subject to alternating magnetic fields. Assuming a particle size below the single-domain limit, we use a macrospin approach and solve the Landau-Lifshitz-Gilbert equation coupled to the mechanical torque equation. Despite its simplicity the presented model exhibits surprisingly rich physics and enables a detailed analysis of the different loss processes depending on field parameters and initial arrangement of the particle and the field. Depending on those parameters regions of different steady states emerge: a region with dominating magnetic relaxation and high magnetic losses and another region region with high frictional losses at low fields or low frequencies. The energy increases continuously even across regime boundaries up to frequencies above the viscous relaxation limit. At those higher frequencies the steady state can also depend on the initial orientation of the particle in the external field. The general behavior and special cases and their specific absorption rates are compared and discussed.

DOI: 10.1103/PhysRevB.107.054416

I. INTRODUCTION

The versatile properties of magnetic fluids are very attractive for applications in biomedicine, for example as contrast agents, in drug targeting or for hyperthermia [1–6]. The magnetic characteristics of the fluid stem from the suspended single-domain magnetic nanoparticles (MNP). Depending on the requirements for an application the material properties have to be chosen carefully and the field parameters need to be tuned for optimal control and efficiency. For magnetically induced hyperthermia in cancer treatment the requirement is to generate as much heat as necessary to destroy cancer tissue. For this procedure, a magnetic fluid suspension is injected intratumoral or close to the cancer cells. Then an alternating magnetic field (AMF) can be used to induce heat in the magnetic fluid by stimulating the MNPs and locally destroy the cancer cells [5,7].

The heat induced inside an MNP by a magnetic AC field is explained by two processes, the Brownian relaxation [8] and Néel relaxation [9], and is generated by surface friction and internal switching of the magnetization. Both processes occur simultaneously and by analyzing the energy losses due to friction and magnetic hysteresis, the heating of the single-domain MNP in a viscous fluid can each be individually quantified with the simulation model presented in this paper.

Studying the heating properties of MNPs with experiments [10–12] and simulations [13–19] is a very active field of research. Usov *et al.* [13] and Usadel *et al.* [14] developed numerical approaches with a system of coupled kinetic equations. They found that the behavior of a particle depends on the field parameters and found two steady states in the zero-temperature case. Furthermore, the influence of temperature on the system is a major point in their paper.

In contrast, in our paper the energy dissipation of a magnetic particle under athermal conditions is studied. Although the thermal fluctuations of the system have been omitted, the self-consistent solution of the coupled magnetization and mechanical dynamics exhibit rich physics. A large parameter study of the field is conducted and dependencies are discussed in a comprehensive fashion. The influences and individual contributions of magnetic and viscous relaxation are analyzed in detail. The emerging two steady states depend on the dominating relaxation process and lead to turning of the particle or allow for the switching of the magnetization. Moreover, while the two steady states can be separated into two regions in the parameter space of field strength and frequency, we also observed a third region depending on the initial orientation of the particle's easy axis relative to the field axis.

In Sec. II the model and methods to calculate the energy losses as well as other comparison models are introduced. The results of the different models and interpretation of such will be discussed in Sec. III. A conclusion is drawn in the last Sec. IV.

*santiago.helbig@univie.ac.at

II. MODEL

Our system consists of a single-domain MNP in a viscous carrier fluid. The particle is assumed to be spherical with an uniaxial crystalline anisotropy. This effectively gives the particle, although spherically symmetrical, a preferred axis of the magnetic moment, which is also referred to as the anisotropy axis or easy axis. In the absence of any external influence, the magnetization is relaxed and resides in the easy axis of the particle. When applying an external magnetic field that is not aligned with the easy axis, the magnetic moment of the particle will decouple from the easy axis in a manner that is defined by the Landau-Lifshitz-Gilbert (LLG) equation [20,21]. The misalignment of the magnetization and the easy axis exerts a mechanical torque rotating the particle. This effect is called Brownian relaxation and will lead, again, to an alignment of the magnetic moment and easy axis with the external field after some transient time.

Néel and Brownian relaxation together with their respective time scales are defined for nonzero temperatures. In this paper the effects of temperature on the system are omitted and are thus instead called magnetic and viscous relaxation respectively.

The equation of motion of the magnetization is defined by the Landau-Lifshitz-Gilbert equation

$$\dot{\boldsymbol{m}} = -\frac{\mu_0\gamma}{1+\alpha^2}\boldsymbol{m}\times\boldsymbol{H}_{\text{eff}} - \frac{\alpha\mu_0\gamma}{1+\alpha^2}\,\boldsymbol{m}\times(\boldsymbol{m}\times\boldsymbol{H}_{\text{eff}}), \quad (1)$$

where $\boldsymbol{m}$ denotes the unit vector in direction of the magnetization, α is the Gilbert damping constant, μ_0 denotes the vacuum permeability, γ denotes the gyromagnetic ratio of the electron $\gamma \approx 1.76 \times 10^{11}$ [$\text{s}^{-1}\text{T}^{-1}$], and the effective field $\boldsymbol{H}_{\text{eff}}$. The effective field can be derived from the energy differential of the total magnetic energy density. The main contributions to the total magnetic energy density are the Zeeman, exchange, demagnetization, and crystalline anisotropy energy. In the macrospin-model only the anisotropy field $\boldsymbol{H}_{\text{ani}}$ and external field $\boldsymbol{H}_{\text{ext}}$ are considered in the effective field

$$\boldsymbol{H}_{\text{eff}} = \boldsymbol{H}_{\text{ani}} + \boldsymbol{H}_{\text{ext}}, \quad (2)$$

where the external field $\boldsymbol{H}_{\text{ext}}$ is an alternating sinusoidal field, and the uniaxial crystalline anisotropy field is given by

$$\boldsymbol{H}_{\text{ani}} = \frac{2K_u}{\mu_0 M_s}(\boldsymbol{m}\cdot\boldsymbol{n})\boldsymbol{n}, \quad (3)$$

with the anisotropy constant K_{u}, the material specific saturation magnetization M_{s}, and the unit vector $\boldsymbol{n}$ assigned to a direction of the easy axis of the particle.

Additionally, the Barnett field $\boldsymbol{H}_{\text{B}}$ has to be included in the effective field $\boldsymbol{H}_{\text{eff}}$ in the damping term of Eq. (1) to account for the rotation of the particle and expand the equation to suit low viscosity fluids [22]

$$\boldsymbol{H}_{\text{B}} = -\frac{\dot{\boldsymbol{\phi}}}{\mu_0\gamma}. \quad (4)$$

$\dot{\boldsymbol{\phi}}$ denotes the angular velocity vector of the particle. Due to high viscosity the magnetization dynamics are much faster than the rotation of the particle resulting in a very low effect of the Barnett field, such that it can be omitted for this paper.

The mechanical equation of motion of the particle, defined by the rotation of its easy axis $\boldsymbol{n}$, can be derived from the conservation of angular momentum and Newton's laws. The total angular momentum of the particle consists of the inertial angular momentum and the angular momentum related to the magnetization [22]

$$\boldsymbol{J} = \boldsymbol{L}_{\text{inert}} + \boldsymbol{L}_{\text{spin}}. \quad (5)$$

The angular momentum of the magnetic moment reads

$$\boldsymbol{L}_{\text{spin}} = -\frac{M_s V_m}{\gamma}\boldsymbol{m}, \quad (6)$$

where V_m denotes the magnetic volume.

The angular momentum of inertia of a sphere rotating around its axis is given by

$$\boldsymbol{L}_{\text{inert}} = \frac{2}{5}m_\star\, r^2\dot{\boldsymbol{\phi}} = \frac{2}{5}\rho\, V r^2\dot{\boldsymbol{\phi}}. \quad (7)$$

In this equation $m_\star$ refers to the mass of the particle and the radius of the particle r. It is denoted with a star and rewritten as the product of density ρ and volume V in order to highlight the dependence on the volume and to avoid any confusion with the magnetic moment $\boldsymbol{m}$.

An external field applies a driving torque to the system and simultaneously a viscous torque decelerates the rotation of the particle leading to changes in the angular momenta that have to be compensated to conserve the total angular momentum $\dot{\boldsymbol{J}} = \boldsymbol{0}$. The torque from the external field reads

$$\boldsymbol{\tau}_{\text{mag}} = \mu_0 M_s V_m \boldsymbol{m}\times\boldsymbol{H}_{\text{ext}}. \quad (8)$$

The standard hydrodynamic result for the viscous torque $\boldsymbol{\tau}_{\text{visc}}$ of a spherical object is given by

$$\boldsymbol{\tau}_{\text{visc}} = -8\pi r^3\eta\,\dot{\boldsymbol{\phi}} = -6V\eta\,\dot{\boldsymbol{\phi}}, \quad (9)$$

with the dynamic viscosity of the carrier fluid η.

This results in a balance of external torques and changes of the internal angular momenta

$$\dot{\boldsymbol{L}}_{\text{spin}} + \dot{\boldsymbol{L}}_{\text{inert}} = \boldsymbol{\tau}_{\text{mag}} + \boldsymbol{\tau}_{\text{visc}} \quad (10)$$

$$-\frac{M_s V_m}{\gamma}\dot{\boldsymbol{m}} + \frac{2}{5}\rho\, V r^2\ddot{\boldsymbol{\phi}} = \mu_0 M_s V_m \boldsymbol{m}\times\boldsymbol{H}_{\text{ext}} - 6V\eta\,\dot{\boldsymbol{\phi}},$$

with the angular acceleration vector $\ddot{\boldsymbol{\phi}}$. Note that the LLG can be inserted in $\dot{\boldsymbol{m}}$.

After rearrangement of the terms, an expression for $\ddot{\boldsymbol{\phi}}$ can be found that results in the mechanical equation of motion of the particle

$$\ddot{\boldsymbol{\phi}} = \frac{5}{2}\frac{\boldsymbol{\tau}_{\text{mag}} + \boldsymbol{\tau}_{\text{visc}} - \dot{\boldsymbol{L}}_{\text{spin}}}{\rho V r^2}, \quad (11)$$

$$\ddot{\boldsymbol{\phi}} = \frac{5}{2}\frac{\mu_0 M_s V_m \boldsymbol{m}\times\boldsymbol{H}_{\text{ext}} - 6V\eta\,\dot{\boldsymbol{\phi}} + \frac{M_s V_m}{\gamma}\dot{\boldsymbol{m}}}{\rho V r^2}. \quad (12)$$

The mixed notation of angular velocity $\dot{\boldsymbol{\phi}}$ and changing rate of vector $\dot{\boldsymbol{m}}$ is useful for determining the energy losses in the next section.

When inserting the LLG into Eq. (12) the magnetic torque cancels partially in the precession term such that the

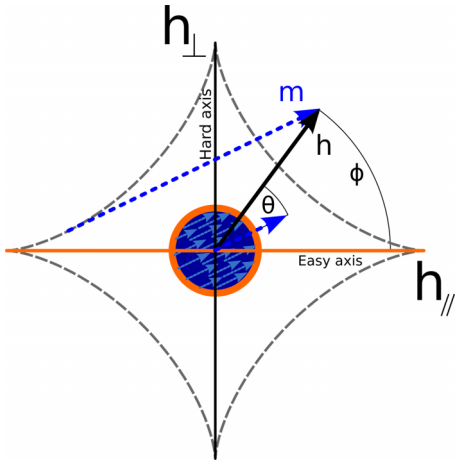

FIG. 1. The Stoner-Wohlfarth astroid. The orange horizontal line indicates the orientation of the easy axis. The black arrow H indicates the applied field, with an angle ϕ relative to the easy axis, while the long blue arrow M draws a tangent on the astroid to the tip of the field vector H, which gives the orientation of the magnetic moment of the particle. It is indicated by the short blue arrow, with angle θ relative to the field, drawn parallel to the long blue arrow at the center.

expression can be rewritten as

$$\ddot{\boldsymbol{\phi}} = \frac{5}{2\rho V r^2}\left[\frac{\mu_0 M_s V_m}{1+\alpha^2}(-\boldsymbol{m}\times\boldsymbol{H}_{\text{ani}} - \alpha\,\boldsymbol{m}\times(\boldsymbol{m}\times\boldsymbol{H}_{\text{eff}}) + \alpha^2\boldsymbol{m}\times\boldsymbol{H}_{\text{ext}}) - 6V\eta\,\dot{\boldsymbol{\phi}}\right]. \tag{13}$$

For $\alpha \ll 1$ the damping term and precession due to the external field vanish. The remaining torque exerted by the anisotropy field on the magnetic moment can be derived from the internal energy of the system [13,23]. Alternatively, omitting the angular momentum of the macrospin leads to a simplified expression of the mechanical equation of motion that does not conserve angular momentum but is faster to compute. But crucially all different expressions are equivalent when in equilibrium such as at low frequencies and when the magnetization is not switching. Furthermore, the viscous torque is overdamping the system justifying those simpler approaches in some cases.

Unless another torque is acting on the particle, the rotation of the particle is more or less confined to a two-dimensional plane apart from the small precession of the magnetization. This plane is spanned by the initial direction of the easy axis and the field axis. The behavior of the particle is symmetric around the field axis.

For the simulations the coordinate system is build such that the field is aligned with the x axis of the coordinate system and the easy axis is located in the x-z plane with some initial angle ϕ relative to the field (see Fig. 1).

For the numerical time integration of the system the following nine-dimensional state vector $\boldsymbol{x}$ and its time derivative $\frac{d}{dt}\boldsymbol{x}$ are used

$$\boldsymbol{x} = \begin{bmatrix}\boldsymbol{m}\\ \boldsymbol{n}\\ \dot{\boldsymbol{\phi}}\end{bmatrix} \quad \frac{d}{dt}\boldsymbol{x} = \begin{bmatrix}\text{RHS of Eq. 1}\\ \dot{\boldsymbol{\phi}}\times\boldsymbol{n}\\ \text{RHS of Eq. 12}\end{bmatrix}, \tag{14}$$

where the update of the direction of the easy axis can be calculated by $\dot{\boldsymbol{n}} = \dot{\boldsymbol{\phi}}\times\boldsymbol{n}$.

Due to the high stiffness of this system the implicit Runge-Kutta scheme, the Radau solver from the *scipy*-library, with adaptive time steps is used in the simulations. The absolute and relative error tolerance was chosen to be 10^{-5} and 10^{-8} respectively. The adaptive time steps are important to join together the two different time scales of the mechanical and magnetic dynamics especially the switching of the magnetization. The data is returned at 100 000 equally-spaced time steps per period for integration of the hysteresis loops.

A. Energy losses

For magnetic systems the dissipated energy of the system can be calculated with help of the hysteresis loop. In the steady state the hysteresis loops will be closed and the area of the hysteresis loop over a cycle c times the magnetic volume V_m of the particle results in the dissipated energy per period [8],

$$E_{\text{tot}} = -\mu_0 V_m \oint_c \boldsymbol{M}(\boldsymbol{H}_{\text{ext}})\, d\boldsymbol{H}_{\text{ext}}. \tag{15}$$

This is equal to the total work performed on the magnetic particle.

The magnetic losses can be determined from the energy dissipation of the magnetization dynamics [24]

$$E_{\text{mag}} = V_m \oint_c \frac{\partial E}{\partial \boldsymbol{m}}\,\dot{\boldsymbol{m}}\, dt. \tag{16}$$

By using the reciprocity theorem this equation and identifying the $\frac{\partial E}{\partial \boldsymbol{m}} = -\mu_0 M_s \boldsymbol{H}_{\text{eff}}$, the effective field, the equation can then be rewritten to match Eq. (15) but considering the effective field instead of only the external field

$$E_{\text{mag}} = -\mu_0 V_m \oint_c \boldsymbol{M}\, d\boldsymbol{H}_{\text{eff}}. \tag{17}$$

As a consequence of Eq. (2), the friction losses can then be calculated by considering only the anisotropy field

$$E_{\text{fric}} = \mu_0 V_m \oint_c \boldsymbol{M}\, d\boldsymbol{H}_{\text{ani}}. \tag{18}$$

Additionally, the angular velocity can be determined from the state of the particle, which allows for the calculation of the viscous torque and an alternative calculation of the dissipated friction energy per cycle

$$E_{\text{fric}} = -\oint_c \boldsymbol{\tau}_{\text{visc}}\,\dot{\boldsymbol{\phi}}\, dt. \tag{19}$$

A constant high angular velocity thus maximizes the friction. Due to the symmetry of the anisotropy and the nature of the AMF, the arc of the rotation is not a full circle but a half circle with acceleration and deceleration as the field alternates. Thus, the particle cannot maintain a constant angular velocity throughout a cycle of the field. For an AMF the optimal conditions occur when the particle is close to the viscous relaxation limit and the particle can remain in motion with short acceleration and deceleration phases.

We will also use the power dissipation per mass $m_\star$, the specific absorption rate SAR, which is an important measure

of heating efficiency for magnetic hyperthermia

$$P_{\mathrm{SAR}} = E_{\mathrm{total}} \frac{f}{m_\star}. \tag{20}$$

Here, f denotes the frequency of the AMF and $m_\star$ denotes the mass of the particle.

B. Comparison models

The hybrid method, which has been developed in this paper, merges two other methods, the immobilized and rigid method. The hybrid solution is simulated with a nonmagnetic surfactant layer, which is necessary for bio-compatibility in medical applications and to prevent aggregation of the particles, additionally the bulk solution, where the whole particle volume is magnetized, is also shown. This leads to a stronger magnetic torque and thus higher angular velocities. For the hybrid solutions the magnetization is not strictly bound to the easy axis, but at small field strengths the decoupling of the magnetization from the easy axis is seemingly minuscule. Still, this small deviation is expected to represent a more realistic scenario.

The immobilized method refers to the immobilization of the easy axis, for example, by increasing the viscosity or enclosing the particle in a solid material, which then only allows for motion of the magnetization and thus is a solely magnetic system. This can be described exactly by the Stoner-Wohlfarth model for frequencies much smaller than the gyromagnetic ratio. The particle's easy axis is fixated in its position and only the magnetization moves relative to the easy axis. The solution of the Stoner-Wohlfarth model has to match the results of the simulated magnetic relaxation.

On the other hand, the rigid solution is a mechanical system, where the magnetic moment is strictly bound to the easy axis. Thus the whole particle rotates like a compass needle to align with the magnetic field. The full equation of motion of the hybrid model can only be solved by means of numerical simulations. However, in the limiting case of very high magnetic anisotropy and omitting inertial effects the system reduces to the mechanical equation of motion, which allows for an analytical solution.

We assume the magnetic and viscous torques scale equally with the size of the particle while the inertial torque at this scale is many magnitudes smaller and can be neglected [25]. This means that inertial effects stop immediately once a force or torque stops acting on the body. When the complete particle can be magnetized then $V_m = V$, omitting the surfactant layer, the system of equations can be further simplified to a size- and mass-independent model with only the scalar magnetic Eq. (8) and viscous torque Eq. (9),

$$\dot{\phi}\,(t) = -\frac{\mu_0 M_{\mathrm{s}} H \sin(\phi) \sin(2\pi f t)}{6\,\eta}, \tag{21}$$

where $\dot{\phi}$ denotes the angular velocity and ϕ the angle of the easy axis and the magnetization relative to the field. The cross product in Eq. (8) has been replaced by $\sin\phi$ for the scalar magnetic torque. H is the maximum field amplitude of the external applied field and η is the viscosity of the fluid. This first order ODE can be analytically solved, which results in

$$\phi(t) = 2\cot^{-1}(e^{k-\mu_0 M_{\mathrm{s}} H \cos(2\pi f t)/(12\eta\pi f)}). \tag{22}$$

Because the magnetic moment of the particle cannot decouple from its easy axis, one angle ϕ is enough to describe the orientation of both easy axis and magnetic moment. The integration constant k can be determined by the initial condition for ϕ.

$$k(\phi_0) = \ln\left(\tan\left(\frac{\pi - \phi_0}{2}\right)\right) + \frac{\mu_0 H M_s}{6\eta}\frac{1}{2\pi f}. \tag{23}$$

In order to compare different calculation methods the initial angle is chosen to be $\phi_0 = \phi(t = 0) = \pi/2$. This leads to the integration constant

$$k = \mu_0 M_{\mathrm{s}} H/(12\eta\pi f). \tag{24}$$

The five different models, the hybrid model with and without a surfactant layer, the rigid model and its analytic solution and the immobilized model will be discussed in the next section.

III. RESULTS

For simplicity we consider the limit of infinite dilution of the magnetic fluid and simulate one spherical uniaxial single-domain MNP suspended in a viscous fluid. The particle is made out of a magnetite-like metal with a *saturation magnetization* $M_{\mathrm{s}} = 400000\,\mathrm{A}/m$, a *density* $\rho = 5170\,\mathrm{kg}/m^3$ and an *anisotropy constant* $K_{\mathrm{u}} = 30000\,\mathrm{J}/m^3$. This yields a anisotropy field of $H_{\mathrm{ani}} \approx 120\,\mathrm{kA}/m$. The particle is spherical with a *radius* $r = 9\,\mathrm{nm}$ and an additional *surfactant layer* $hs = 1\,\mathrm{nm}$. The surfactant layer is considered nonmagnetic and mass-less (much less dense than the magnetic core of the particle) and therefore only contributes to the viscous torque by increasing the surface friction and damping the movement of the particle. The surrounding carrier fluid has the *dynamic viscosity parameter* $\eta = 0.89\,\mathrm{mPa}$, which corresponds to the viscosity of water at 20 °C. The dimensionless Gilbert *damping parameter* is chosen to be $\alpha = 0.08$. For the simulations the parameters are kept mostly consistent and any deviations from our standard values will be highlighted. The simulations are run for 100 cycles of the AMF, which should be enough time for the particle to settle in a steady state even at frequencies above the viscous relaxation limit. The particle settles in fewer cycles in its steady state for lower frequencies.

Concerning the characteristic time scales, at body temperature of 37 °C ≈ 310 K and for a radius of 10 nm the Brownian relaxation time is about $\tau_{\mathrm{B}} \approx 2.6\,\mu s$. This means that the Brownian relaxation limit is reached at ≈400 kHz. This value is close to the viscous relaxation limit. The viscous limit τ_R varies stronger because it is field strength dependent but it is of a similar magnitude as the Brownian relaxation limit τ_B with a limit between 10 μs and 0.6 μs. The switching time τ_S in our model is about a thousand times shorter than the viscous relaxation time of the particle. The Néel relaxation time for the magnetic core of radius 9 nm for a temperature of 310 K is $\tau_{\mathrm{n}} \approx 4\,\mathrm{s}$. This suggests high stability of the magnetic state and the prevention of the superparamagnetic behavior [26]. In a first comparison of the five different calculation models,

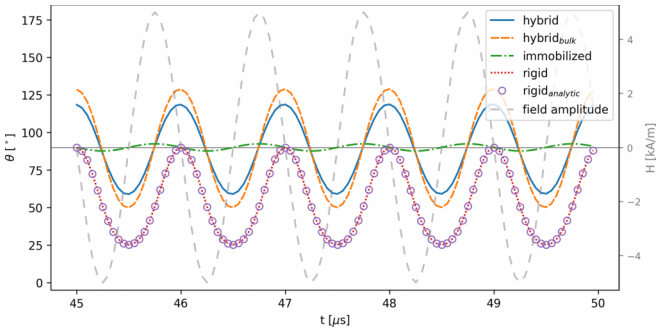

FIG. 2. Plot of the oscillation of θ in time. Taken for different initial configurations for a particle with 10 nm radius, a field strength of 5 kA/m and a frequency of 100 kHz, the trajectories are compared. Here shown: with decoupled magnetization and a surfactant layer (*hybrid*), when completely magnetized and no surfactant layer (*hybrid*$_{\text{bulk}}$), for the magnetic system (*immobilized* easy axis), for the mechanical system (*rigid*) and the *analytic* solution. The dashed light-gray line indicates the amplitude of the field. The initial angle for all systems was $\phi_0 = 90°$.

the behavior of the orientation of magnetization is shown in Fig. 2.

A. Dynamics of a mechanical system

Reducing our model to a system of mechanical equations leads to the rigid method. For the rigid$_{\text{analytic}}$ and rigid solution the results show periodic behavior, but the particle's rotation is very stiff. The particle's movement is only rotating into the direction of the initial extension of the field and then back to its initial position, see Fig. 2. For high frequencies, much higher than the viscous relaxation limit, and low field strengths the hybrid method and analytical solution match well due to the limited rotation of the magnetization and easy axis and the reduced magnetic torque. The particle in the hybrid model for field strengths lower than half the anisotropy field strength will usually oscillate perpendicular to the field axis.

At low frequencies, when the particle aligns with the field, it does so in an exponential fashion [see Eq. (22)]. A close alignment of the particle with the field leads to very small values for ϕ and can lead to mismatches of the analytic solution and in the time evolution of the rigid model due to numerical inaccuracies. Thus, the results match better at low fields when the particle is unable to completely relax via viscous relaxation and align with the field. On the other hand, especially at higher frequencies and strong fields the magnetic relaxation dominates for finite anisotropy and the results of the analytic solution would no longer suffice as an approximation.

Unsurprisingly, this approach cannot exhibit any magnetic losses and all the losses have to be due to friction. But in this case the anisotropy field $\boldsymbol{H}_{\text{ani}}$ is always zero and the effective field $\boldsymbol{H}_{\text{eff}}$ is always equal to the external field $\boldsymbol{H}_{\text{ext}}$. Equations (15) and (17) are thus identical while Eq. (18) is always zero. Therefore, Eq. (19) can be used to calculate the friction losses and verify the result of the total losses Eq. (15).

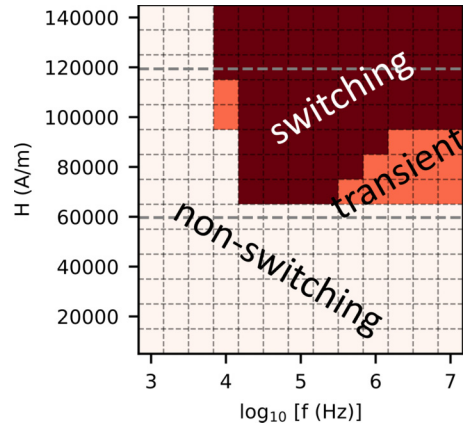

FIG. 3. Showing the region of magnetic reversal in the parameter space of field strength and frequency. In the dark region (*switching*) the particle always settles into a switching steady state. This means the magnetization will continuously switch in the steady state according to the oscillation of the AMF. In the *transient* region the steady state depends on the initial angle between easy axis and field. The particle rotates without the switching of the magnetization in the light region (*nonswitching*). The horizontal dashed lines indicate half (≈60 kA/m) and the full anisotropy field (≈120 kA/m).

B. Dynamics of a solely magnetic system

This system only accounts for magnetic losses and is represented by the immobilized solution, where the easy axis is unable to rotate. In Fig. 2, the magnetization is highly restricted in its motion because of the immobilized easy axis and the magnetization cannot deviate too much from the easy axis due to the high anisotropy constant. In contrast to the Stoner-Wohlfarth-model, the angular velocity of the magnetic moment is finite and does not relax instantaneously. A mismatch of the results at high frequencies can be expected.

For an immobilized particle the magnetic losses are completely independent of the frequency until it starts to approach the magnetization switching limit τ_S. The energy output is the same as the particle will always switch at the same field strength leading to the same hysteresis losses. This system is not adjustable as it either dissipates no energy or it always outputs the same energy.

C. Dynamics of the fully-coupled hybrid system

The two prior models show the behavior in the limit of no friction and high friction to the point of immobilization of the particle. Friction depends on the viscosity of the medium, which determines the viscous relaxation time. Thus, the two models also represent the limits for frequencies well below and far above the viscous relaxation time. Depending on the choice of material parameters and field strength, this leads to two distinct regions and a transient region of steady states, see Fig. 3.

The variety of steady states can be fundamentally subdivided into two categories: switching and nonswitching. The regions indicate for which field parameters the magnetic moment flips or the particle rotates to accommodate for the change in field intensity. The parameter space can be further

divided by the anisotropy field strength, half the anisotropy field strength and the viscous relaxation limit for frequencies.

For an immobilized particle, the dissipated energy depends highly on the initial angle as predicted by the Stoner-Wohlfarth model but is generally independent of the frequency. Magnetic relaxation can also be influenced by the rotation of the particle. A rigid particle, on the other hand, gets limited strongly by the viscous relaxation limit and thus has a lower energy output for higher frequencies. Characteristics of both models will still appear in the hybrid method. Such as its two possible steady states that are quite similar to both previously mentioned models and their steady states. The magnetization-switching behavior of the hybrid method is similar to the solely magnetic system, while the nonswitching steady case is reminiscent of the rigid model.

In order to observe the particle transitioning to a steady state, where it reliably switches the orientation of magnetization, the Stoner-Wohlfarth model [27] can be utilized. The Stoner-Wohlfarth astroid (see Fig. 1) indicates that, depending on the alignment of field and easy axis, between half and the full anisotropy field H_{ani} [see Eq. (3)] strength has to be at least applied in order to switch the magnetization. The minimum switching field can switch the magnetization at an angle of exactly 45° between the field and easy axis. Since the particle is also simultaneously rotating, this strict angle cannot be maintained. Thus, the particle starts switching its magnetization at a slightly higher critical field strength than half the anisotropy field strength. Above 100 kHz the conditions are optimal for the magnetization to switch at the weakest field strength, which is about 65 kA/m or about 0.54 H_{ani}. Upon reaching the viscous relaxation limit the rotation of the easy axis is slowed down by the increasing viscous torque. A similar critical field strength for the transition has also been found by Usadel *et al.* [14] and Coene *et al.* [28]. The transition to the switching phenomena can thus be generally observed between 65 kA/m and 120 kA/m. In order to cover this transition region and also study the low field strength regime, a range from 1 kA/m to 140 kA/m is chosen.

As a side note, if easy axis and magnetization are perfectly aligned with the field, the magnetization will actually not start switching, because at that point the system is perfectly balanced. Due to thermal fluctuations this situation should not occur in experiments. In the simulations the symmetry needs to be broken by very small perturbations to the initial angle. As previously mentioned, the hysteresis curve for the external field represents the total energetic losses due to magnetic and viscous relaxation during a cycle of the AMF. For field strengths below half the anisotropy field strength H_{ani} it is impossible for the magnetization to switch and thus only allows the particle to relax via viscous relaxation. For intermediate field strengths, between half and the full anisotropy field, it depends on the field frequency. The hysteresis area seems to increase monotonically with the field strength at low frequencies but its shape seems to change as well. If the magnetization does not switch, the shape is more rounded while at higher field strengths, due to the switching of the magnetization, the corners become sharp, see Fig. 4. The switching leads to a sudden change in magnetization. Afterwards the particle continues to relax slightly via viscous relaxation as well. Although time is not resolved in the hysteresis loop, the

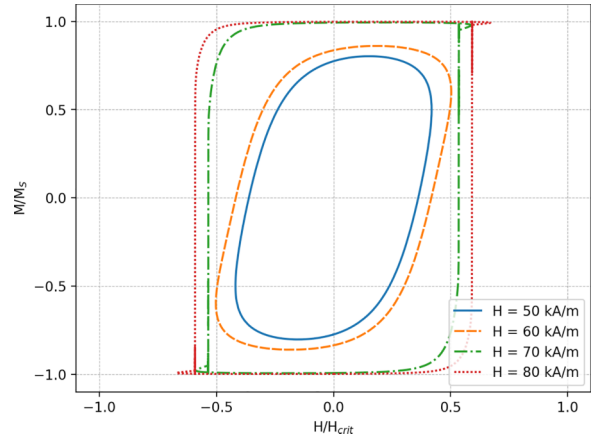

FIG. 4. The hysteresis curve in the global frame of reference of an MNP during a steady state cycle of the AMF for four different field strengths (50 kA/m to 80 kA/m from the inside to the outside) at 500 kHz. The particle is simulated with the default parameters. The simulation includes mechanical rotation and therefore the curve captures both mechanical and magnetic processes. M/M_{s} corresponds to the alignment of the magnetization with the field. Full saturation is reached when the magnetization is completely aligned with the field.

difference in time scale for rotation [Eq. (A2)] and magnetization switching [Eq. (A3)] means that the particle spends significantly more time relaxing with viscous relaxation, even though the switching of the magnetization is mostly responsible for the energy dissipation. The area of the hysteresis loops in Fig. 4 increases abruptly at high frequencies when increasing the field strength and transitioning from viscous to mostly magnetic relaxation. For the lower field strengths the particle does not reach saturation M/M_{s}, which means that it is not able to fully relax via viscous relaxation and the field is too weak to cause the magnetization to switch via magnetic relaxation. For stronger fields the magnetic relaxation might also not lead to a relaxed state at very high frequencies that approach the magnetization switching limit $1/\tau_S$. No matter the field parameters, the hysteresis loops as seen in Fig. 4 are always closed.

While magnetic losses can mainly occur if the magnetization switches, friction, although very limited, is always present. And even if no full relaxation is possible, rotation of the easy axis, albeit marginal, still occurs. The particle will settle in a steady state of the least energy losses and leads to an oscillation with small amplitude perpendicular to the field axis. For weak field strengths the magnetic moment does not deviate too far from the easy axis, which results in a small magnetic torque and an almost motionless easy axis. This will be further discussed in Sec. III E.

The frequency of the AMF thus is also crucial in determining the behavior of the particle and relates to the time scales of the viscous and magnetic relaxation. In the simulations a range 1–10 MHz is chosen because for medical applications the frequencies are rather low [11] but this range also shows the transition from viscous to a dominating magnetic relaxation and at higher frequencies also the emergence of a configuration that depends on the initial arrangement of

easy axis and field (see "transient region" in Fig. 3). Low frequencies allow for effective viscous relaxation, where the easy axis can align with the field axis in positive and negative x direction as the field alternates. On rare occasion the particles magnetization can switch for intermediate field strengths (60 kA/m to 120 kA/m). These spontaneous switching events may stem from the length of the time-step and could be avoided with a higher time resolution. Increasing the frequency of the field closer to the viscous relaxation limit, contrary to the previous case, sometimes the particle is too well aligned with the field such that the magnetization does not switch at all and remains motionless for one or more cycles of the field. For slightly higher frequencies the previous inconsistencies vanish completely and for stronger field strengths the magnetic relaxation becomes the preferred relaxation mechanism.

As the viscous relaxation limit is approached, the frictional losses reach their maximum. Although energy dissipation in the switching region is mainly dominated by magnetic relaxation, at these frequencies there is also still a noticeable effect of viscous relaxation. Energy losses due to magnetization switching are independent of the frequency, thus the additional friction contribution leads to the maximum in total energy losses per cycle. Above the viscous relaxation limit the losses due to friction drop off and for frequencies, for which the inverse approaches the magnetization switching time, the magnetization will be unable to completely relax but the frequencies in our simulations are lower than this threshold.

Figure 5 shows that the friction losses persist even at high frequencies where magnetic losses dominate, but shrink as the frequency increases. In the limit of high frequencies the system approaches the state of a solely magnetic system for which the surrounding fluid acts as a solid matrix at such high frequencies. Still, the deflection of the magnetic moment from the easy axis leads to a nonzero torque on the easy axis due to the anisotropy and a rotation of the particle and thus to nonzero friction losses at all frequencies and field strengths.

These influences of frequency and field are depicted in Fig. 6. In three plots of the space of field parameters, the magnetic (a), friction (b), and combined losses (c) are shown.

Even when computing the friction losses by integrating the viscous torque and the angular velocity [see Eq. (19)], the sum of viscous and magnetic losses calculated with Eq. (17) matches the total losses Eq. (15) up to a small difference. Because of this mutual agreement we concluded that the hysteresis loops are closed and correctly describe the total losses. The difference shown in Fig. 7 is calculated by

$$\Delta E = \frac{100}{E_{\text{total}}}(E_{\text{total}} - E_{\text{mag}} + E_{\text{fric}}). \tag{25}$$

The difference is very small (<0.2%). The simulation results are evaluated for 100 000 equidistant time steps per period in order to obtain high numerical accuracy.

Including the inertia in the equation of motion Eq. (12) is important and leads to a different energy landscape although inertial effects should be negligible at such high viscosity. But without the inertial term and the spin angular momentum the particle has lower energy dissipation at lower frequencies where viscous relaxation dominates and the particle starts to prefer magnetic switching at higher frequencies, see Fig. 5. Thus we conclude that the dynamic equilibrium of the coupled system is more susceptible to inertial effects. Only omitting the spin angular momentum does not have the same impact.

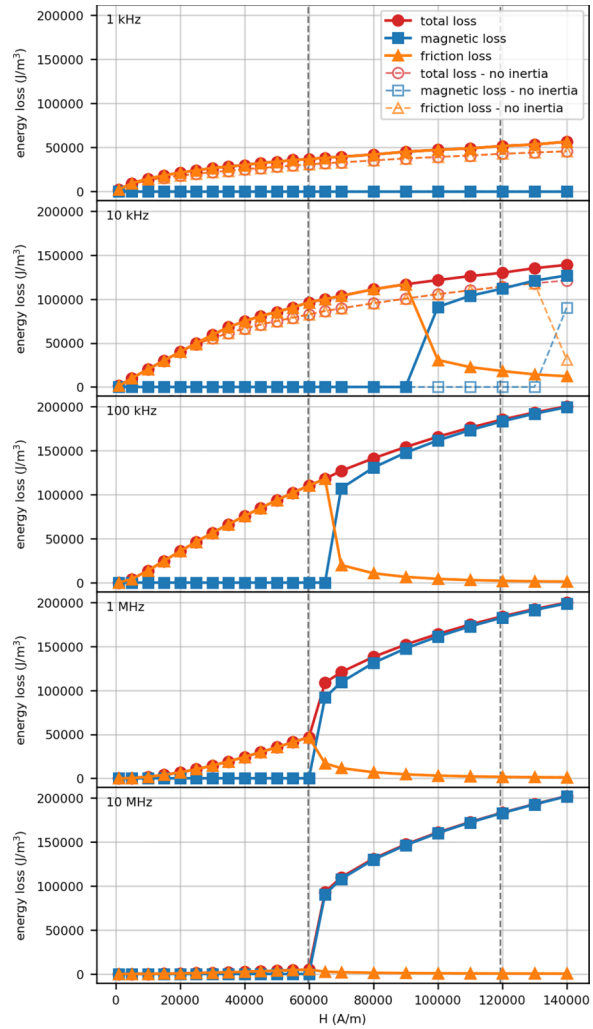

FIG. 5. The energy loss contributions of magnetic and friction processes for some sample of frequencies (increasing frequencies from top to bottom). The losses for calculations without inertia are also included in a paler shade and with dashed lines.

The behavior of the particle is also influenced by other parameters such as the saturation magnetization, the anisotropy and the shape and size of the particle. The anisotropy field strength is defined by the anisotropy constant and the saturation magnetization, see Eq. (3). The saturation magnetization and the field strength equally contribute to the calculation of H_{ani} and thus the results for varying the field strength can be analogously applied to variation of the saturation magnetization.

The anisotropy energy is also a determining factor for the stability of the magnetization when exposed to thermal influences. Fortunately, the anisotropy energy of the particle in the simulations is 30 kJ/m^3 and thus rather high. Together with the relatively large size of the particle this results in high stability against thermal fluctuations and the superparamagnetic behavior is avoided.

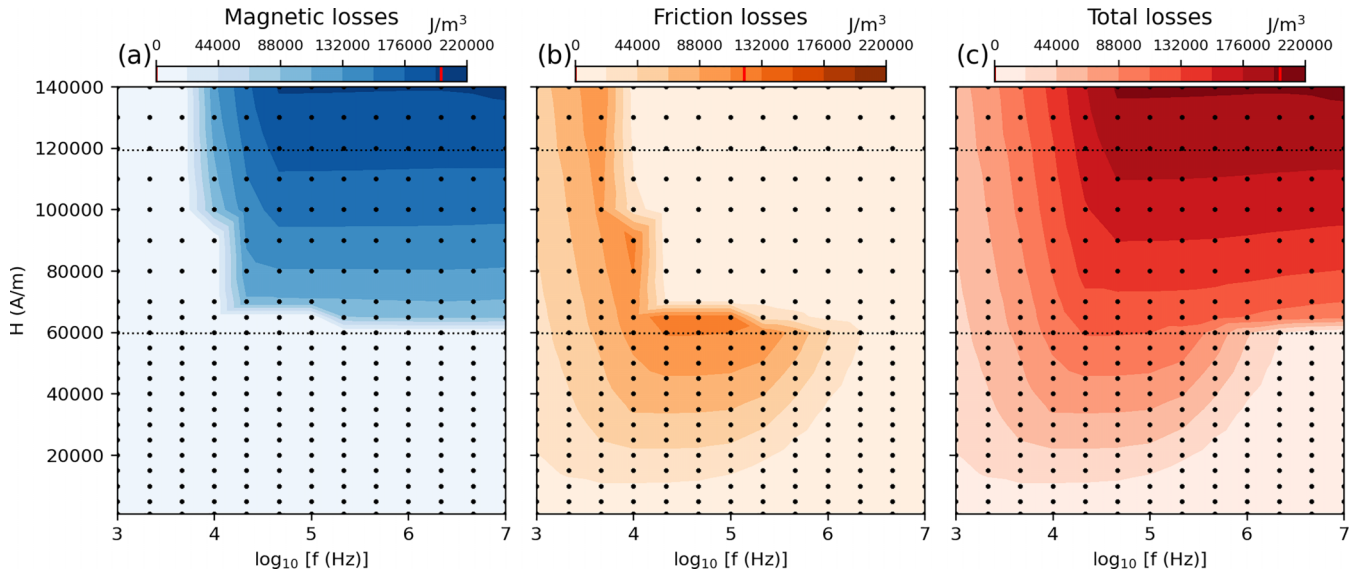

FIG. 6. The energy losses as generated by magnetic processes (a), friction (b), and the total losses (c) in the space of the field parameters. The data points are logarithmically scaled according to the frequency. The values are taken for an initial angle $\phi_0 = 45^\circ$. The indicator lines in the color bars show the minimum and maximum energy value. The color gradients follow the same logarithmically scaling. Thin gray lines at 60 kA/m and 120 kA/m indicate half and full anisotropy field strength respectively.

Apart from the field and material parameters, the fluid also influences the dynamic behavior of the particle. The fluid is primarily defined by its viscosity, which limits the angular rotation of the particle and is a determining factor for friction and the viscous relaxation time. Increasing the viscosity leads to switching of the magnetic moment at lower frequencies, that is, it shifts the switching domain to lower frequencies, while in the high viscosity limit it approaches the solely magnetic model discussed in Sec. III B. The specific absorption rate SAR (see Fig. 8) is the most important result for hyperthermia in order to quantify the heating properties of the magnetic fluid and defined as the dissipated power per unit mass, see Eq. (20). In general, the SAR increases with field strength and frequency. Noticeably for low field strengths (<30 kA/m) the SAR value drops off because of an insufficient magnetic torque and for frequencies above the viscous relaxation limit the SAR value remains almost constant.

D. Initial angle dependency—The transient region

Because of the dependency of the anisotropy field strength H_{ani} on the angle ϕ between easy axis and field in the

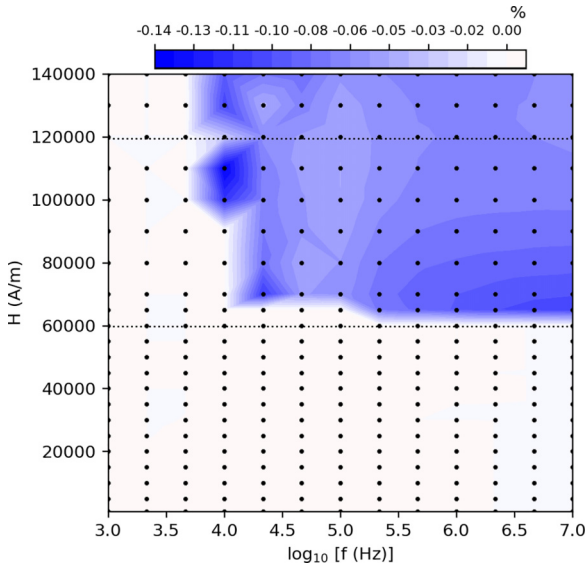

FIG. 7. The difference of calculating the total energy loss per cycle directly via the hysteresis or as the sum of magnetic losses and frictional losses from the angular velocity [see Eq. (19)] shown as a color gradient. These results are taken from simulations with an initial angle $\phi_0 = 45^\circ$.

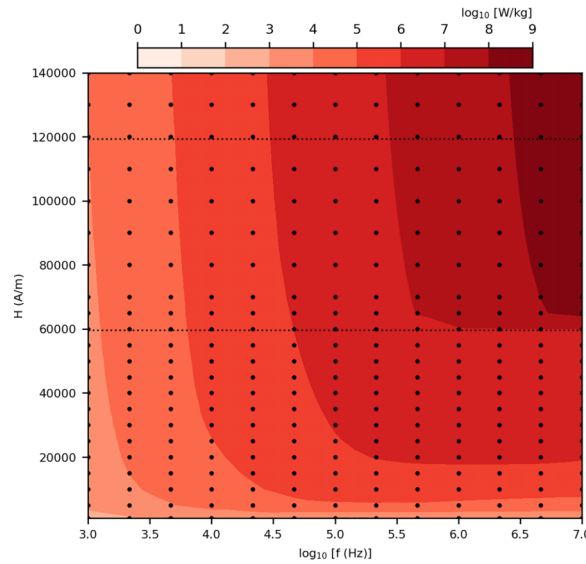

FIG. 8. The specific absorption rate (SAR) in a phase space diagram with logarithmic color scaling. The values are taken for an initial angle $\phi_0 = 45^\circ$.

Stoner-Wohlfarth model (see Fig. 1) we were interested to see if there are any differences in behavior of the particle depending on the initial angle. In general, every initial angle ϕ_0 will result in the same steady state after a transient phase of a few cycles of the AMF. Since the motion of the particle is confined in a plane the results are also symmetric around the field axis. During the cycles of the transient phase the particle can also change its behavior from switching to nonswitching or vice versa until it settles in the steady state.

If the field is slightly stronger than half the anisotropy field strength H_{ani} then, at frequencies exceeding the viscous relaxation limit, two steady states can emerge for the same combination of field strength and frequency. Depending on the initial angle the particle can either switch its magnetization or enter a niche steady state of oscillation shown in Fig. 3 as "transient" region where the magnetization does not switch and the particle oscillates perpendicular to the field axis. In case of obtuse initial angles ($90^\circ - 180^\circ$) the behavior is similar to simulations with lower field strengths without magnetization switching. This is unusual since at intermediate field strengths $0.5H_{\text{ani}} < H_{\text{ext}} < H_{\text{ani}}$ the steady state should be a state of switching of the magnetization. This range of angles inhibiting the magnetization switching widens at higher frequencies.

Since these simulations do not consider interactions between particles or the temperature, and therefore thermal activation of the magnetization switching, this nonswitching steady state might be too fragile to occur in experiments. Previously balanced states could become less stable if temperature is included and the special case of steady states that depend on the initial angle could vanish.

At 10 kHz and high field strengths the steady state is not completely stable and relaxation can alternate in the simulations between switching and nonswitching of the magnetization contrary to the "transient" region. Thus, at the boundary of the two regimes the steady state is not clearly defined and stands out in Figs. 3 and 7.

E. Amplitude and average angle of oscillation

At the nanoscale the inertial effects are generally small such that the easy axis cannot overshoot or perform a full rotation during one cycle of an AMF. The maximum amplitude of the rotation of the easy axis is 180° aligning once in positive and negative x direction with the field axis. For low field strengths and frequencies above the viscous relaxation limit the amplitude shrinks drastically (see Fig. 9). Although the particle can rotate for small field strengths, it turns very slowly and thus does not dissipate that much energy due to friction.

In general, if the particle's magnetization does not switch then it oscillates from 0° to 180° resulting in an average angle of 90°, shown in numbers in Fig. 9) for low frequencies. The average angle remains the same even as the amplitude of oscillation decreases due to the viscous relaxation limit as the frequency increases. For very weak fields at high frequencies the magnetic torque is almost negligible and the easy axis will remain close to its initial orientation, only oscillating slightly.

On the other hand, for fields exceeding the anisotropy field strength the magnetization usually switches and the easy axis remains close to the field with a very small amplitude and an average angle close to 0°. This holds true in general for high field strengths, except for frequencies well below the viscous relaxation limit, where the particle usually does not switch.

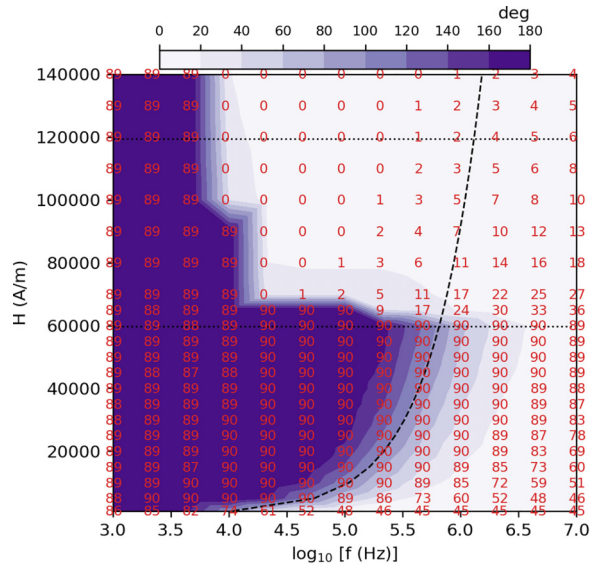

FIG. 9. The amplitude of the rotation of the easy axis as a gradient in degrees and the average angle of that oscillation written in numbers during one cycle of the AMF both given in degrees. The dashed curve indicates the viscous relaxation limit. The initial angle in the simulations is $\phi_0 = 45^\circ$.

IV. CONCLUSIONS

The framework developed in this paper provides the foundation of an elaborate simulation model for magnetic fluids. By understanding the inner mechanisms of the particles in the fluid, more sophisticated predictions about the behavior of the fluid can be derived. Moreover, our model can show various interesting effects of a magnetic nanoparticle in a fluid, that simpler models cannot capture. Although for specific cases simpler models may suffice, better results are usually obtained by the hybrid method, even though the computational cost is slightly higher. With the mechanical motion derived from the conservation of angular momentum and the LLG solving the magnetization dynamics inside of the particle, it has been shown for which configuration of field parameters the simulated particle settles in a switching or nonswitching steady state. Another transient region in the space of field parameters in which the steady state depends on the initial angle between field and easy axis has also been observed and discussed.

Using the hysteresis curves to visualize the change and the underlying calculations for the energy losses clearly indicate the transition of the heating mechanisms and the total energy losses. The total dissipated energy increases continuously even as the system transitions from the nonswitching to the switching steady state. At higher frequencies this transition is more abrupt due to the viscous relaxation limit and the reduced frictional losses. The magnetic hysteresis losses remain mostly independent of the frequency since they are caused by the irreversible switching of the magnetization,

which depends mostly on the field strength. For that reason, the maximum energy losses are achieved when the viscous relaxation can be maximized as viscous relaxation is always present. This maximum total energy loss is reached shortly before reaching the viscous relaxation limit at around 100 kHz. The behavior of the easy axis and the magnetization have been thoroughly discussed and the results solidify this model as a model to study the physics of a magnetic fluid.

The SAR value has been found to increase monotonously with increasing field and frequency, however, for very low field strengths and frequencies over the viscous relaxation limit the SAR value remains almost constant.

Our future studies will focus on the further variation of the material and fluid parameters. This includes the shape of the particle, which could introduce an additional anisotropy factor and would also change the viscous torque on the particle. And although for the simulations the viscosity of water was chosen in this paper, a more realistic fluid would be blood (at 37 °C), which is more viscous. Furthermore, thermal fluctuations not only influence the magnetization but can also change the size of the particle and the viscosity of the fluid and will be necessary to include in further studies.

ACKNOWLEDGMENTS

The authors wish to thank the "FWF - Der Wissenschaftsfonds" for funding under the Project No. P 33748 and the Vienna Scientific Cluster (VSC) for providing the necessary computational resources. We acknowledge financial support by the Vienna Doctoral School in Physics (VDSP). P.A.S. acknowledges support from the project "Computer modeling of magnetic nanosorbents", funded by the University of the Balearic Islands and the European Regional Development Fund. This research has been partially performed in the framework of the RSF Project No.19-12-00209.

APPENDIX A: CHARACTERISTIC TIME SCALES

An important metric to estimate the influence of the mechanical and magnetic dynamics and their influence on the power loss is given by the characteristic relaxation time connected to the respective process. The Brownian relaxation time τ_B is defined as the following:

$$\tau_B = \frac{3\eta V}{k_B T}, \tag{A1}$$

here η denotes the dynamic viscosity, V is the hydrodynamic volume of the MNP, k_B is the Boltzmann constant, and T is the temperature of the system.

Due to the zero-temperature approach in this paper, an alternative description for the rotation limit can be derived from setting the magnetic torque Eq. (8) equal to the viscous torque Eq. (9) and by rewriting $\dot{\phi} = \omega = 2\pi/\tau_R$ and maximizing it. This yields the viscous relaxation time

$$\tau_R = \frac{12\pi V \eta}{\mu_0 M_S V_m H}, \tag{A2}$$

which gives the limit for the rotation depending on the field strength.

The time it takes for the magnetization to switch its orientation via the LLG Eq. (1) is given by [29]

$$\tau_S = \frac{2}{\mu_0 \gamma H} \frac{1+\alpha^2}{\alpha}. \tag{A3}$$

The magnetization switching time is much shorter than the viscous relaxation limit.

The Néel relaxation time τ_N is the average lifetime of the magnetic state in absence of an external field and is derived from the Néel-Arrhenius law [9]

$$\tau_N = \tau_0 \exp\left(\frac{K_u V_m}{k_B T}\right). \tag{A4}$$

τ_0 is the so-called attempt time and denotes the time frame that the magnetization should remain stable. In this case, the inverse of the frequency of the AMF marks the attempt time since the particles magnetization should not switch due to thermal fluctuations for the duration of at least one cycle. The relaxation time is defined by the ratio of the anisotropy energy of the particle $K_u V_m$ and the thermal energy $k_B T$.

APPENDIX B: MAGNETIZATION SWITCHING FIELD STRENGTH

In the analysis of energy losses, the field strength necessary to switch the magnetization has to be considered. The astroid derived from the Stoner-Wohlfarth model [27] (see Fig. 1) allows to geometrically determine the orientation of the magnetic moment when an external magnetic field is applied. The astroid itself also indicates the field strength that is necessary to switch the magnetization in the particle. The required field strength to overcome the anisotropy barrier is the anisotropy field H_{ani} see Eq. (3). Sharrock [30] derived an elaborate method to analyze the thermal influence on the switching fields

$$H_S = H_{\text{SW}} \left\{ 1 - \left[\left(\frac{k_B T}{K_u V_m} \right) \ln \frac{t}{\tau_N} \right]^n \right\}, \tag{B1}$$

where n is a factor dependent on the angle between the field and the easy axis. Setting the temperature T to zero yields a coercive field same as the switching field of Stoner-Wohlfarth H_{SW}. Thus, in the limit of 0 K temperature our model holds true. For finite temperatures the anisotropy field strength overestimates the critical switching field.

[1] E. A. Périgo, G. Hemery, O. Sandre, D. Ortega, E. Garaio, F. Plazaola, and F. J. Teran, Fundamentals and advances in magnetic hyperthermia, Appl. Phys. Rev. **2**, 041302 (2015).

[2] E. Pollert, G. Goglio, S. Mornet, and E. Duguet, Magnetic nanoparticles for magnetic resonance imaging and hyperthermia applications, in *Nanomaterials: A Danger or a Promise?* (Springer, New York, 2013) pp. 99–129.

[3] Q. A. Pankhurst, J. Connolly, S. K. Jones, and J. Dobson, TOPICAL REVIEW: Applications of magnetic nanoparticles in biomedicine, J. Phys. D: Appl. Phys. **36**, R167 (2003).

[4] C. S. Kumar and F. Mohammad, Magnetic nanomaterials for hyperthermia-based therapy and controlled drug delivery, Adv. Drug Delivery Rev. **63**, 789 (2011).
[5] B. Thiesen and A. Jordan, Clinical applications of magnetic nanoparticles for hyperthermia, Int. J. Hyperthermia **24**, 467 (2008).
[6] I. M. Obaidat, B. Issa, and Y. Haik, Magnetic properties of magnetic nanoparticles for efficient hyperthermia, Nanomaterials **5**, 63 (2015).
[7] R. R. Baker, C. Payne, Y. Yu, M. Mohseni, J. J. Connell, F. Lin, I. F. Harrison, P. Southern, U. S. Rudrapatna, D. J. Stuckey *et al.*, Image-guided magnetic thermoseed navigation and tumor ablation using a magnetic resonance imaging system, Adv. Sci. **9**, 2105333 (2022).
[8] W. F. Brown, *Micromagnetics*, Interscience Tracts on Physics and Astronomy 18 (Interscience Publishing, New York, 1963).
[9] L. Néel, Théorie du traînage magnétique des ferromagnétiques en grains fins avec applications aux terres cuites, Ann. géophys. **5**, 99 (1949).
[10] S. Dutz and R. Hergt, Magnetic nanoparticle heating and heat transfer on a microscale: Basic principles, realities and physical limitations of hyperthermia for tumour therapy, Int. J. Hyperthermia **29**, 790 (2013).
[11] W. J. Atkinson, I. A. Brezovich, and D. P. Chakraborty, Usable frequencies in hyperthermia with thermal seeds, IEEE Trans. Biomed. Eng. **BME-31**, 70 (1984).
[12] S. Dutz, R. Hergt, J. Mürbe, R. Müller, M. Zeisberger, W. Andrä, J. Töpfer, and M. Bellemann, Hysteresis losses of magnetic nanoparticle powders in the single domain size range, J. Magn. Magn. Mater. **308**, 305 (2007).
[13] N. Usov and B. Y. Liubimov, Dynamics of magnetic nanoparticle in a viscous liquid: Application to magnetic nanoparticle hyperthermia, J. Appl. Phys. **112**, 023901 (2012).
[14] K. D. Usadel and C. Usadel, Dynamics of magnetic single domain particles embedded in a viscous liquid, J. Appl. Phys. **118**, 234303 (2015).
[15] S. Ruta, R. Chantrell, and O. Hovorka, Unified model of hyperthermia via hysteresis heating in systems of interacting magnetic nanoparticles, Sci. Rep. **5**, 9090 (2015).
[16] O. Hovorka, J. Barker, G. Friedman, and R. W. Chantrell, Role of geometrical symmetry in thermally activated processes in clusters of interacting dipolar moments, Phys. Rev. B **89**, 104410 (2014).
[17] J. Carrey, B. Mehdaoui, and M. Respaud, Simple models for dynamic hysteresis loop calculations of magnetic single-domain nanoparticles: Application to magnetic hyperthermia optimization, J. Appl. Phys. **109**, 083921 (2011).
[18] Y. L. Raikher and V. Stepanov, Physical aspects of magnetic hyperthermia: Low-frequency ac field absorption in a magnetic colloid, J. Magn. Magn. Mater. **368**, 421 (2014).
[19] H. Mamiya and B. Jeyadevan, Hyperthermic effects of dissipative structures of magnetic nanoparticles in large alternating magnetic fields, Sci. Rep. **1**, 157 (2011).
[20] L. D. Landau and E. M. Lifshitz, Theory of the dispersion of magnetic permeability in ferromagnetic bodies, Phys. Z. Sowjetunion **8**, 153 (1935).
[21] T. L. Gilbert, A phenomenological theory of damping in ferromagnetic materials, IEEE Trans. Magn. **40**, 3443 (2004).
[22] H. Keshtgar, S. Streib, A. Kamra, Y. M. Blanter, and G. E. W. Bauer, Magnetomechanical coupling and ferromagnetic resonance in magnetic nanoparticles, Phys. Rev. B **95**, 134447 (2017).
[23] Y. Raikher and M. Shliomis, The effective-field method in the orientational kinetics of magnetic fluids and liquid-crystals, Adv. Chem. Phys **87**, 595 (1994).
[24] C. Abert, Micromagnetics and spintronics: Models and numerical methods, Eur. Phys. J. B **92**, 120 (2019).
[25] E. M. Purcell, Life at low Reynolds number, Am. J. Phys. **45**, 3 (1977).
[26] C. P. Bean and J. D. Livingston, Superparamagnetism, J. Appl. Phys. **30**, S120 (1959).
[27] E. C. Stoner and E. P. Wohlfarth, A Mechanism of Magnetic Hysteresis in Heterogeneous Alloys, Phil. Trans. R. Soc. Lond. A **240**, 599 (1948).
[28] A. Coene and J. Leliaert, Simultaneous coercivity and size determination of magnetic nanoparticles, Sensors **20**, 3882 (2020).
[29] H. Kronmüller, General micromagnetic theory, Handbook of Magnetism and Advanced Magnetic Materials (2007).
[30] M. Sharrock, Time dependence of switching fields in magnetic recording media, J. Appl. Phys. **76**, 6413 (1994).